

Relativistic self-consistent mean-field description of Sm isotopes

Afaque Karim* and Shakeb Ahmad†

Physics Department, Aligarh Muslim University, Aligarh 202002, India

(Received 14 July 2015; revised manuscript received 23 October 2015; published 22 December 2015)

The evolution of the shape from the spherical to the axially deformed shapes of the neutron-rich, even-even $^{144-164}\text{Sm}$ transitional nuclei is investigated. The investigations are performed with explicit density-dependent meson-nucleon and point-coupling models within the framework of the covariant density functional theory. A nonlinear meson-nucleon coupling model represented by the NL3* parametrization of the relativistic mean-field Lagrangian has also been used. The bulk and the microscopic properties of these nuclei have been investigated to analyze the phase-transition region and the critical-point behavior. The microscopic and self-consistent quadrupole deformation-constrained calculations show a clear shape change for even-even Sm isotopes with $N = 82-102$. The potential energy surfaces for ^{148}Sm , ^{150}Sm , and ^{152}Sm obtained using different interactions are found to be relatively flat, which may be the possible critical-point nuclei. By examining the single-particle spectra, it is found that these nuclei distribute more uniformly as compared to other isotopes. Investigations also support the proposed shell-closure properties of ^{162}Sm . Overall good agreement is found within the different models used and between the calculated and experimental results wherever available.

DOI: [10.1103/PhysRevC.92.064608](https://doi.org/10.1103/PhysRevC.92.064608)

PACS number(s): 27.70.+q, 21.60.Jz, 21.30.Fe, 21.10.Pc

I. INTRODUCTION

Among finite many-body systems, atomic nuclei are prime examples of deformed quantum systems [1–5]. Dynamical symmetries related to atomic nuclei provide an elegant analytic framework for understanding their characteristics [6]. In fact, most nuclei cannot be represented by the limiting cases of pure symmetries. Rather, they are located in a region of shape transitions where the dynamical symmetries break, near the critical point, and deformed shapes evolve as the number of valence nucleons increases. The investigation of shape fluctuations and critical-point behavior in transitional nuclei, as a function of nucleon number, is a hot topic in nuclear-structure analysis [7–17], in spite of the fact that the concept of phase transition is only approximate for finite nuclear systems. Interpretation of the evolution of the structure of such nuclei in the phase transition region has traditionally been a difficult task because they exhibit a complicated interplay of competing degrees of freedom. It is quite challenging to understand and predict the properties of such nuclei at the critical point where structure is changing dramatically. Nevertheless, understanding such nuclei is important because their structure defines the nature of the transition region itself.

The phase transition corresponds to the breaking of the dynamical symmetries. The interacting boson model (IBM) [18] gives three dynamical symmetries—U(5), SU(3), and SO(6)—which corresponds to spherical, axially deformed, and γ -unstable shapes. Based on these symmetries, it has been shown that the phase transition between spherical U(5) and axially deformed shapes SU(3) is of the first order [19,20]. The first exact solvable analytical model for the critical-point system was proposed by Iachello *et al.* [21–23] with the development of a new class of critical-point symmetries which

are based on the analytical solutions of the Bohr-Hamiltonian eigenvalue problem. These dynamical symmetries are denoted by E(5) [22] and X(5) [23]. These describe systems at the critical point of a first-order phase transition in one (deformation β) and two (β and γ) variables, respectively. In the nuclear context, these apply to a shape transition from a spherical to a quadrupole deformed region. Two coexisting minima in the potential surface, a spherical and a deformed one, whose energy difference varies with nucleon numbers, give the idea of X(5) critical-point symmetry. The first example of X(5) symmetry in the transition region from a spherical vibrator to an axial rotor is ^{152}Sm [21,24–28], because it is very near the critical point of this transition region. It also shows evidence of phase coexistence. Transitional nuclei like ^{150}Nd [29] and others in different nuclear transition regions have also been reported [30–37] as examples of X(5) symmetry. Theoretical studies also confirm many transitional nuclei as critical-point nuclei in different phase-transition regions [38–41]. However, there is no assurance that any specific nuclei will be the critical-point nuclei because nuclear properties change discretely with N and Z , as nuclei contain integer numbers of nucleons.

Further, in this context, the study of neutron-rich nuclei becomes important because such nuclei are different from normal nuclei. The new experimental facilities make it possible to investigate these nuclei using rare exotic ion beams. This has stimulated the theoretical study of the nuclear many-body dynamics. From the studies of neutron-rich nuclei, a wealth of structure phenomena has been reported. This includes the following extensive variety of phenomena: the quenching of shell closure [42–46] and the observation of new magic numbers [47–49]; confirmation of the predictions by Brack *et al.* [50] that $Z, N = 38$, and $N = 60$ are new magic numbers with deformed shapes [51,52]; theoretical prediction of new deformed magic numbers such as $N = 100$, $Z \approx 62$, $N = 150$, $Z = 78$, and $N = 164$, $Z \approx 90$ for the island of stability near the drip-line region [53–55]. To predict new magic nuclei and

*afaquekrm@gmail.com

†Corresponding author: physics.sh@gmail.com

an associated island of stability near the drip line, shell effect is important [53,54].

A systematic microscopic investigation of the phase-transition region and critical-point behavior of the transitional nuclei is necessary. It is the best way to address where and how the corresponding dynamical symmetries occur. The relativistic and nonrelativistic models based on effective field theory (EFT) and density functional theory (DFT) are the most tested and successful theoretical models to investigate the properties of atomic nuclei [56–59].

A microscopic and self-consistent mean-field model based on relativistic mean-field (RMF) theory [60] has been successfully applied in the analyses of a variety of nuclear-structure phenomena. They provide an accurate description of ground-state properties and collective excitation of atomic nuclei [61–69]. These models are widely used to analyze from relatively light systems to superheavy nuclei and from the valley of β stability to the particle drip lines. The role of density functional theories in understanding nuclear many-body dynamics is important. This is done in terms of the energy density functionals (EDFs). These functionals are approximated by the self-consistent mean-field models. They include all higher-order correlations, with powers and gradients of ground-state nucleon densities (see Refs. [58,70–73] and references therein). These have been applied successfully, as an exact theory in Coulombic systems [74,75]. The Lagrangian of the current generation of self-consistent mean-field models includes the density-dependent meson-nucleon vertex function. Relativistic models with an explicit density-dependent meson-nucleon and point coupling provide an improved microscopic description of nuclei over standard nonlinear meson self-interactions (see Refs. [71], [72], and [76] and references therein).

However, Lorentz invariance is one of the underlying symmetries of quantum chromodynamics (QCD). Therefore, covariant density functionals [61,72] are of particular interest in a nuclear-physics context, where the situation is much more complicated. Covariant density functionals are very successful in the nuclear-structure studies [77–99] because the strong relativistic fields in the nucleus describing the velocity and spin dependence in an appropriate way, leading to a number of important effects, are automatically reproduced in relativistic calculations. However, in the meantime, the most successful and modern covariant density functionals have been derived [100–104]. These are based on density-dependent vertices and one additional parameter characterizing the range of the force, in particular, the density-dependent meson-exchange DD-ME1 [100], DD-ME2 [101], and DD-PC1 [102] (density-dependent point-coupling) effective interactions. These provide a very successful and an excellent description of different ground states and excited states over the entire periodic table [72,80,101,105,106]. The present paper aims for a better and systematic understanding of the phase-transition region and critical-point concept in transitional nuclei using the microscopic and self-consistent RMF models. The present study shows that $^{144–164}\text{Sm}$ are excellent empirical manifestations of the critical-point structure concept. Even-even samarium (Sm) isotopes have been the focal point of a large number of experimental studies [28,107–111]. Their study is

a challenging theoretical problem, too, because they lie in the range from near-spherical to well-deformed shapes. It is believed that ^{148}Sm is basically spherical, while ^{154}Sm is a well-deformed nucleus, and $^{150–152}\text{Sm}$ are transitional nuclei.

In our present work, the neutron-rich, even-even $^{144–164}\text{Sm}$ nuclei ($Z = 62$) are studied using the newly improved self-consistent RMF models. These consist of a constrained RMF model [60,112–115] with nonlinear meson-nucleon interaction (NL3*) [116] and the covariant density functional models [117]: The density-dependent meson-exchange model (DD-ME) and a density-dependent point-coupling model (DD-PC) are used.

The paper is organized as follows. The theoretical framework and details of the numerical calculations are discussed in Sec. II. The results of the investigations of the ground-state properties, quadrupole deformation, potential energy surface (PES), and single-particle energies are presented in Sec. III. Finally, Sec. IV summarizes the results of our work.

II. THEORETICAL FORMALISM

A. Covariant density functional theory

Covariant density functional theory (CDFT), namely, meson-exchange model (DD-ME) and a point-coupling model (DD-PC), are used in the present calculation. The basic difference between these two models lies on the treatment of the interaction range, the mesons, and the density-dependence. DD-ME and DD-PC are density-dependent models but DD-ME has a finite interaction range, while DD-PC uses a zero-range interaction with one additional gradient term in the scalar-isoscalar channel. Each of these models is represented here by its corresponding parameter sets as DD-ME1 [100], DD-ME2 [101], and DD-PC1 [102].

1. Meson-exchange models

Phenomenology of the meson-exchange model considers the nucleus as a system of Dirac nucleons. These nucleons interact via the exchange of mesons with finite masses, leading to a finite-range interaction [101,116,118]. The isoscalar-scalar σ meson, the isoscalar-vector ω meson, and the isovector-vector ρ meson build the minimal set of meson fields for a quantitative description of nuclei. The standard Lagrangian density of the meson-exchange model with medium dependence vertices is written as [115]

$$\begin{aligned} \mathcal{L} = & \bar{\psi} [\gamma(i\partial - g_\omega \omega - g_\rho \vec{\rho} \cdot \vec{\tau} - e\mathbf{A}) - m - g_\sigma \sigma] \psi \\ & + \frac{1}{2}(\partial\sigma)^2 - \frac{1}{2}m_\sigma^2\sigma^2 - \frac{1}{4}\Omega_{\mu\nu}\Omega^{\mu\nu} + \frac{1}{2}m_\omega^2\omega^2 \\ & - \frac{1}{4}\vec{R}_{\mu\nu}\vec{R}^{\mu\nu} + \frac{1}{2}m_\rho^2\vec{\rho}^2 - \frac{1}{4}\mathbf{F}_{\mu\nu}\mathbf{F}^{\mu\nu}, \end{aligned} \quad (1)$$

where m is the bare nucleon mass and ψ denotes the Dirac spinors. The masses m_σ , m_ω , and m_ρ are those of the σ meson, ω meson, and the ρ meson, respectively, with the corresponding coupling constants for the mesons to the nucleons as g_σ , g_ω , g_ρ , respectively, and e is the charge of the proton. These coupling constants and unknown meson masses are parameters of the Lagrangian Eq. (1). Here $\Omega^{\mu\nu}$, $\vec{R}^{\mu\nu}$, and $F^{\mu\nu}$ are the field tensors of the vector fields ω , ρ , and A .

and the photon:

$$\Omega^{\mu\nu} = \partial^\mu\omega^\nu - \partial^\nu\omega^\mu, \quad (2)$$

$$\vec{R}^{\mu\nu} = \partial^\mu\vec{\rho}^\nu - \partial^\nu\vec{\rho}^\mu, \quad (3)$$

$$\mathbf{F}^{\mu\nu} = \partial^\mu\mathbf{A}^\nu - \partial^\nu\mathbf{A}^\mu. \quad (4)$$

In the above expressions, isovectors are denoted by arrows, and boldface symbols are used for vectors in ordinary three-dimensional space. The functions g_σ , g_ω , and g_ρ are assumed to be vertex functions of Lorentz-scalar bilinear forms of the nucleon operators.

From the Lagrangian density, we obtain the Hamiltonian density $\mathcal{H}(\mathbf{r})$ [61], and by integrating it over the \vec{r} space the total energy is obtained, which depends on the Dirac spinors and the meson fields

$$E_{\text{RMF}}[\psi, \bar{\psi}, \sigma, \omega^\mu, \vec{\rho}^\mu, \mathbf{A}^\mu] = \int d^3r \mathcal{H}(\mathbf{r}). \quad (5)$$

This linear model has first been introduced by Walecka [60,112]. However, this simple model, with interaction terms only linear in the meson fields, does not provide a quantitative description of nuclear systems [113,114]. It turns out that a nonlinear self-coupling for scalar mesons,

$$U(\sigma) = \frac{1}{2}m_\sigma^2\sigma^2 + \frac{1}{3}g_2\sigma^3 + \frac{1}{4}g_3\sigma^4, \quad (6)$$

plays a crucial role for a realistic description of complex nuclear-system properties [113]. This model has been successfully used in a number of studies [115,119–121]. Following the idea of Brockmann and Toki [122] to use density-dependent couplings, in the meson-exchange model, the meson-nucleon vertex functions g_σ , g_ω , and g_ρ are determined. It is done by adjusting the parameters of an assumed phenomenological density dependence of meson-nucleon coupling to reproduce the experimental data in finite nuclei [100,101,118,123]. The density dependence of the meson-nucleon couplings is parametrized in a phenomenological approach [100,118,123]. The couplings of the σ meson and the ω meson to the nucleon field are defined as

$$g_i(\rho) = g_i(\rho_{\text{sat}})f_i(x) \quad \text{for } i = \sigma, \omega, \quad (7)$$

where

$$f_i(x) = a_i \frac{1 + b_i(x + d_i)^2}{1 + c_i(x + d_i)^2} \quad (8)$$

is a function of $x = \rho/\rho_{\text{sat}}$ and ρ_{sat} denotes the baryon density at saturation in the symmetric nuclear matter. The eight real parameters in Eq. (8) are not independent, but constrained as follows:

$$f_i(1) = 1, \quad f''_\sigma(1) = f''_\omega(1), \quad f''_i(0) = 0. \quad (9)$$

These five constraints reduce the number of independent parameters to three. Three additional parameters in the isoscalar channel are $g_\sigma(\rho_{\text{sat}})$, $g_\omega(\rho_{\text{sat}})$, and m_σ . The functional form of the density dependence of the ρ -meson coupling is suggested by a Dirac-Brueckner calculations of asymmetric nuclear matter [124]:

$$g_\rho(\rho) = g_\rho(\rho_{\text{sat}})\exp[-a_\rho(x - 1)]. \quad (10)$$

TABLE I. The parameters of the effective interactions DD-ME1 and DD-ME2 in the Lagrangian.

Parameter	DD-ME1 [100]	DD-ME2 [101]
m_σ	549.5255	550.1238
m_ω	783.0000	783.0000
m_ρ	763.0000	763.0000
$g_\sigma(\rho_{\text{sat}})$	10.4434	10.5396
$g_\omega(\rho_{\text{sat}})$	12.8939	13.0189
$g_\rho(\rho_{\text{sat}})$	3.8053	3.6836
a_σ	1.3854	1.3881
b_σ	0.9781	1.0943
c_σ	1.5342	1.7057
d_σ	0.4661	0.4421
a_ω	1.3879	1.3892
b_ω	0.8525	0.9240
c_ω	1.3566	1.4620
d_ω	0.4957	0.4775
a_ρ	0.5008	0.5647

The isovector channel is parametrized by $g_\rho(\rho_{\text{sat}})$ and a_ρ . The eight independent parameters (seven coupling parameters and the mass of the σ meson) were adjusted to reproduce the properties of symmetric and asymmetric nuclear matter, and to ground-state properties of spherical nuclei [125–127]. The present investigation uses the very successful density-dependent meson-exchange relativistic energy functionals DD-ME1 [100] and DD-ME2 [101] given in Table I.

2. Point-coupling model

In complete analogy to the meson-exchange phenomenology, the point-coupling model represents an alternative formulation of the self-consistent RMF framework [102,128–131]. The effective Lagrangian for the density-dependent point-coupling model [102,132] that includes the isoscalar-scalar, isoscalar-vector, and isovector-vector four-fermion interactions is given by

$$\begin{aligned} \mathcal{L} = & \bar{\psi}(i\gamma.\partial - m)\psi \\ & - \frac{1}{2}\alpha_s(\hat{\rho})(\bar{\psi}\psi)(\bar{\psi}\psi) - \frac{1}{2}\alpha_V(\hat{\rho})(\bar{\psi}\gamma^\mu\psi)(\bar{\psi}\gamma_\mu\psi) \\ & - \frac{1}{2}\alpha_{TV}(\hat{\rho})(\bar{\psi}\vec{\tau}\gamma^\mu\psi)(\bar{\psi}\vec{\tau}\gamma_\mu\psi) \\ & - \frac{1}{2}\delta_S(\partial_\nu\bar{\psi}\psi)(\partial^\nu\bar{\psi}\psi) - e\bar{\psi}\gamma \cdot \mathbf{A} \frac{1 - \tau_3}{2}\psi. \end{aligned} \quad (11)$$

It contains the free-nucleon Lagrangian, the point-coupling interaction terms, and the coupling of the proton to the electromagnetic field. The derivative terms in Eq. (11) account for the leading effects of finite-range interactions that are crucial for a quantitative description of the nuclear properties. The functional form of the point couplings chosen is

$$\alpha_i(\rho) = a_i + (b_i + c_i x)e^{-d_i x}, \quad (i = S, V, TV), \quad (12)$$

where $x = \rho/\rho_{\text{sat}}$ and ρ_{sat} denote the nucleon density at saturation in the symmetric nuclear matter. In the present work, we have used the recently developed density-dependent

TABLE II. The parameters of the effective interaction DD-PC1 in the Lagrangian.

Parameter	DD-PC1 [102]
m	939
a_σ	-10.046 16
b_σ	-9.150 42
c_σ	-6.427 29
d_σ	1.372 35
a_ω	5.919 46
b_ω	8.863 70
d_ω	0.658 35
b_ρ	1.835 95
d_ρ	0.640 25

point-coupling interaction DD-PC1 [102] given in Table II. Treatment of the pairing correlations has been carried out as described in Ref. [117].

The study of PES as a function of the quadrupole deformation parameter is performed by the method of quadratic constraint [133]. In the present calculation, we restrict ourselves to axially symmetric configurations with reflection symmetry. The method of quadratic constraint uses an unrestricted variation of the function

$$\langle \hat{H} \rangle + \sum_{\mu=0,2} C_{2\mu} (\langle \hat{Q}_{2\mu} \rangle - q_{2\mu})^2, \quad (13)$$

where $\langle \hat{H} \rangle$ is the total energy, $\langle \hat{Q}_{2\mu} \rangle$ denotes the expectation values of mass quadrupole operators

$$\hat{Q}_{20} = 2z^2 - x^2 - y^2 \quad \text{and} \quad \hat{Q}_{22} = x^2 - y^2, \quad (14)$$

$q_{2\mu}$ is the constrained value of the multipole moment, and $C_{2\mu}$ is the corresponding stiffness constant [133]. Moreover, the quadratic constraint adds an extra force term $\sum_{\mu=0,2} \lambda_\mu \hat{Q}_{2\mu}$ to the system, where $\lambda_\mu = 2C_{2\mu}(\langle \hat{Q}_{2\mu} \rangle - q_{2\mu})^2$ is for a self-consistent solution. This term is necessary to force the system to a point in deformation space different from a stationary point. The augmented Lagrangian method [134] has also been implemented to resolve the problem of convergence of the self-consistent procedure. It diverges while increasing the value of stiffness constant $C_{2\mu}$ used in the procedure.

B. Axially deformed relativistic mean-field model

The RMF theory [60] has received wide attention because of its successful description of many nuclear phenomena during the past year [61]. The effective Lagrangian density considered [60,113–115] is written in the form

$$\begin{aligned} \mathcal{L} = & \bar{\psi}_i \{i\gamma^\mu \partial_\mu - M\} \psi_i + \frac{1}{2} \partial^\mu \sigma \partial_\mu \sigma - \frac{1}{2} m_\sigma^2 \sigma^2 \\ & - \frac{1}{3} g_2 \sigma^3 - \frac{1}{4} g_3 \sigma^4 - g_s \bar{\psi}_i \psi_i \sigma - \frac{1}{4} \Omega^{\mu\nu} \Omega_{\mu\nu} \\ & + \frac{1}{2} m_w^2 V^\mu V_\mu + \frac{1}{4} c_3 (V_\mu V^\mu)^2 - g_w \bar{\psi}_i \gamma^\mu \psi_i V_\mu \end{aligned}$$

TABLE III. The parameters of the effective interaction NL3* in the Lagrangian.

Parameter	NL3* [116]
m	939
m_σ	502.5742
m_ω	782.600
m_ρ	763.0000
g_σ	10.0944
g_ω	12.8065
g_ρ	4.5748
g_2	-10.8093
g_3	-30.1486
c_3	0.0

$$\begin{aligned} & - \frac{1}{4} \vec{B}^{\mu\nu} \cdot \vec{B}_{\mu\nu} + \frac{1}{2} m_\rho^2 \vec{R}^\mu \cdot \vec{R}_\mu - g_\rho \bar{\psi}_i \gamma^\mu \vec{\tau} \psi_i \cdot \vec{R}^\mu \\ & - \frac{1}{4} F^{\mu\nu} F_{\mu\nu} - e \bar{\psi}_i \gamma^\mu \frac{(1 - \tau_{3i})}{2} \psi_i A_\mu. \end{aligned} \quad (15)$$

It describes the nucleons with the mass M as Dirac spinors ψ moving in the fields of σ , ω , and ρ mesons and the Coulomb field. The field tensors $\Omega^{\mu\nu}$, $\vec{R}^{\mu\nu}$, and $F^{\mu\nu}$ are given in Eq. (4). From the above Lagrangian, we obtain the Dirac equation for the nucleons and the Klein-Gordon-type equations for mesons and the photon. These equations are solved by expanding the above and lower components of Dirac spinors and the boson fields in an axially deformed harmonic oscillator basis with an initial deformation β_0 . The set of coupled equations is solved numerically by a self-consistent iteration method. The center-of-mass energy correction is estimated by the usual harmonic oscillator formula $E_{cm} = \frac{3}{4}(31A^{-1/3})$. The quadrupole deformation is evaluated from the resulting proton and neutron quadrupole moments as $Q = Q_n + Q_p = \sqrt{\frac{16\pi}{5}}(\frac{3}{4\pi} AR^2 \beta_2)$. The root-mean-square (rms) matter radius is defined as $\langle r_m^2 \rangle = \frac{1}{A} \int \rho(r_\perp, z) r^2 d\tau$, where A is the mass number, and $\rho(r_\perp, z)$ is the deformed density. The total binding energy and other observables are also obtained by using the standard relations, given in Refs. [114,115]. For the nuclei studied in this work, the optimum basis is taken into account to produce a good convergence on the binding energy and deformation in the numerical calculations. We have used the recently proposed parameter set NL3* [116] given in Table III, which is a modern version of the widely used parameter set NL3 [120]. It improves the description of the ground-state properties of many nuclei over parameter set NL3 and provides simultaneously excellent description of excited states with collective character in spherical as well as deformed nuclei.

Pairing calculation

It is well known that pairing correlations have to be included in any realistic calculation of medium and heavy nuclei. In principle, the microscopic Hartree-Fock-Bogoliubov (HFB) theory should be used, which have been developed in several papers [57,61,72,77,100–102,104,105,116,120,135–138] and

the references given there. However, for pairing calculations of a broad range of nuclei not too far from the β -stability line, a simpler approach, the constant gap, BCS pairing approach is reasonably well. However, this simple approach breaks down for nuclei far from the valley of β stability where the coupling to the continuum is important [139]. In the present study we treat pairing correlations using the BCS approach. Although the BCS approach may fail for light neutron-rich nuclei, the nuclei considered here is not light neutron-rich nuclei and the RMF results with the treatment should be reliable.

The contribution of the pairing interaction to the total energy for each nucleon is

$$E_{\text{pair}} = -G \left[\sum_{i>0} u_i v_i \right]^2, \quad (16)$$

where v_i^2 and $u_i^2 = 1 - v_i^2$ are the occupation probabilities and G is the pairing force constant [114,115,140,141]. The variational procedure with respect to the occupation numbers v_i^2 gives the BCS equation

$$2\varepsilon_i u_i v_i - \Delta(u_i^2 - v_i^2) = 0, \quad (17)$$

and the gap Δ is defined by

$$\Delta = G \sum_{i>0} u_i v_i. \quad (18)$$

This is the famous BCS equation for pairing energy. The densities are contained within the occupation number

$$n_i = v_i^2 = \frac{1}{2} \left[1 - \frac{\varepsilon_i - \lambda}{\sqrt{(\varepsilon - \lambda)^2 + \Delta_k^2}} \right]. \quad (19)$$

For the pairing gaps for proton and neutron, we choose the standard expressions. It is valid for nuclei both on and away from the stability line, which are given by the following expressions [142]:

$$\Delta_p = RB_s e^{-sI-tI^2/Z^{1/3}}, \quad (20)$$

$$\Delta_n = RB_s e^{-sI-tI^2/A^{1/3}}. \quad (21)$$

The inputs of pairing gaps, i.e., $R = 5.72$, $s = 0.118$, $t = 8.12$, $B_s = 1$, and $I = (N - Z)/(N + Z)$, have been used in nuclear physics for many years; we consider that they are suitable here. The occupation probability is calculated using Eqs. (20) and (21). The chemical potentials λ_n and λ_p are determined by the particle numbers of neutrons and protons. Using Eqs. (18) and (19) the pairing energy for nucleon can be written as

$$E_{\text{pair}} = -\frac{\Delta^2}{G} = -\Delta \sum_{i>0} u_i v_i. \quad (22)$$

It can be seen from Eq. (22) that the pairing energy E_{pair} is not constant because it depends on the occupation probabilities v_i^2 and u_i^2 , and hence on the deformation parameter β_2 , particularly near the Fermi surface. It is known to us that the pairing energy E_{pair} diverges if it extended to an infinite configuration space for a constant pairing gap parameter Δ and

force constant G . Also, for the states spherical or deformed, with large momenta near the Fermi surface, it decreases in all realistic calculations with finite range forces. However, for the sake of simplicity of calculation, we have taken the constant pairing gap. It is assumed that the pairing gaps for all the states are equal to each other near the Fermi surface. In the present calculation, we have used a pairing window, and all the equations extended up to the level $\varepsilon_i - \lambda \leq 2(41A^{1/3})$. A factor of 2 has been included to reproduce the pairing correlation energy of neutrons in ^{118}Sn using the Gogny force [114,115,140].

The PES map as a function of quadrupole deformation parameter is obtained microscopically by the constrained RMF theory with reflection symmetry. The binding energy is obtained at a certain deformation by constraining the quadrupole moment $\langle Q_2 \rangle$ to a given value μ_2 in the expectation value of the Hamiltonian [133]

$$\langle H' \rangle = \langle H \rangle + \frac{1}{2} C_\mu (\langle Q_2 \rangle - \mu_2)^2, \quad (23)$$

where C_μ is the constraint multiplier. The deformation parameter β_2 is obtained from the calculated quadrupole moments $\langle Q_2 \rangle$ for the protons and neutrons through

$$\langle Q_2 \rangle = \langle Q_{2n} \rangle + \langle Q_{2p} \rangle = \sqrt{\frac{16\pi}{5}} \left(\frac{3}{4\pi} AR^2 \beta_2 \right). \quad (24)$$

III. RESULTS AND DISCUSSION

A. Ground-state properties

There exist a number of nonrelativistic and relativistic parameter sets for solving the standard Lagrangian of mean-field models. The ground-state properties, like the binding energies (BEs), quadrupole deformation parameters β_2 , charge radii (r_c), and other bulk properties, are evaluated using these parameter sets. It is found that, more or less, most of the recent parameter set reproduces the ground-state properties, not only of stable, normal nuclei, but also of exotic nuclei far away from the valley of β stability. This means that if one uses a reasonably acceptable parameter set, the predictions of the model will remain nearly force independent. In this paper, the ground-state properties like the BE, quadrupole deformation parameters β_2 , charge radii r_{ch} , and other bulk properties are evaluated using recently available effective interactions. These are density-dependent meson-exchange DD-ME1 [100], DD-ME2 [101], DD-PC1 [102] (density-dependent point-coupling), and nonlinear meson NL3* [116] effective interactions. The present calculations using these interactions produce the ground-state properties for $^{144-164}\text{Sm}$ nuclei and are in excellent agreement with the experimental data available. The different numerical results are compared with the results reported using the self-consistent HFB approximation based on the finite-range and density-dependent Gogny interaction [143] with the parametrization D1S [144]. Comparison with the results reported within the self-consistent HFB + transformed harmonic-oscillator (THO) framework, using the Skyrme SLy4, SkP, and SkM* forces along with the Lipkin-Nagomi (LN) prescription followed by exact particle-number projection (PNP) [145] are also presented here.

TABLE IV. The total BE with CDFT (DD-ME1, DD-M2, DD-PC1) and RMF(NL3*) model for even-even $^{144-164}\text{Sm}$ isotopes are compared with the Skyrme SLy4, SkP, SkM* forces [146] and the experimental values [135,147] wherever available.

E (MeV)	EXP	DD-ME1	DD-ME2	DD-PC1	NL3*	SLy4	SkP	SkM*
^{144}Sm	1195.74	1198.79	1197.30	1198.70	1199.05	1196.23	1194.54	1190.56
^{146}Sm	1210.91	1210.99	1209.47	1210.79	1212.17	1208.16	1209.27	1204.24
^{148}Sm	1225.40	1224.79	1223.34	1224.72	1225.75	1221.18	1223.57	1218.50
^{150}Sm	1239.25	1239.01	1237.67	1239.23	1239.57	1235.25	1237.72	1233.26
^{152}Sm	1253.11	1252.55	1251.55	1253.37	1253.70	1248.77	1251.15	1248.86
^{154}Sm	1266.94	1266.13	1265.42	1267.46	1267.59	1262.84	1264.92	1264.10
^{156}Sm	1279.99	1278.42	1277.64	1280.16	1279.98	1274.76	1277.86	1277.59
^{158}Sm	1291.98	1290.11	1289.40	1292.37	1291.65	1286.17	1289.88	1290.61
^{160}Sm	1303.36	1301.20	1300.65	1304.16	1302.95	1297.03	1301.20	1302.08
^{162}Sm	1313.82	1311.52	1311.04	1314.83	1313.34	1307.54	1311.78	1313.30
^{164}Sm	1323.32	1319.93	1319.61	1324.06	1322.28	1316.31	1321.32	1324.09

More details, including a downloadable table of ground-state properties are available online in Ref. [146]

B. Binding energy, two-neutron separation energy (S_{2n}), rms charge radius r_{ch} , and pairing energy (E_{pair})

Binding energies are important quantities of nuclei and they are directly related to the stability of nuclei and to α -decay energies. Whether a model can quantitatively reproduce the experimental BE is a crucial criterion by which to judge the validity of the model. The BEs of the ground state are listed in Table IV. The constrained calculations are carried out with the density-dependent meson-exchange DD-ME1 [100], DD-ME2 [101], DD-PC1 [102] (density-dependent point-coupling), and nonlinear meson NL3* [116] effective interactions. For the BE the data is well reproduced within 0.2%. Particularly, excellent agreement (within 1 MeV) is obtained for BE in $^{146-164}\text{Sm}$ with DD-ME1, DD-PC1, and NL3*, except in case of DD-ME2, where it is $\sim 0.2\%$. Even for neutron magic nuclei ^{144}Sm , the difference between the calculated results and the experimental data [135,147] is less than 3 MeV, i.e., less than 0.3% relatively. The present numerical results for the BE have been compared with the HFB + THO method with LN correction followed by exact PNP based on the Skyrme SLy4, SkP, and SkM* interactions [146]. The numerical results are in good agreement within $\sim 0.5\%$ among the different self-consistent mean-field approaches using different interactions along with the experimental data [135,147]. In Fig. 1(a), we display the calculated two-neutron separation energy $S_{2n}(N, Z) = \text{BE}(N, Z) - \text{BE}(N - 2, Z)$ along with experimental data [148] wherever possible. A comparison with the macro-microscopic finite-range-droplet model (FRDM) predictions [149] and the predictions with the HFB + THO + LN + PNP method based on the Skyrme SLy4, SkP, and SkM* interactions [146] have also been presented. From the figure, we find that the calculated microscopic S_{2n} values agree well within the experimental data, the macro-microscopic FRDM calculations, and the HFB + THO + LN + PNP results, except with SkM* interaction. We notice that, as we move away from the strong $N = 82$ ($A = 144$) shell closure, the magicity of $Z = 62$ rapidly decreases. Apparently, the S_{2n} decreases gradually with the increase of neutron number, except for the

noticeable kinks at $A = 150$, $A = 154$, $A = 162$ with DD-ME, DD-PC, SLy4, and SkP forces and at $A = 154$ with NL3* and SkM* forces. Macro-microscopic FRDM calculations and experimental values do not show any kinks except at $N = 82$ ($A = 144$) shell closure. Interestingly, we can say that the region between the kinks at $A = 146$ and $A = 154$ suggests the transition region. Also, the kink at $A = 162$ suggests that $N = 100$ as a deformed magic number for ^{162}Sm , supporting some earlier studies [53,54,150,151].

To investigate the point of neutron shell closure characterized by a vanishing neutron pairing energy alone [152,153], we show in Fig. 1(b) the neutron pairing energy $E_{pair,n}$ obtained using covariant density functional approach for Sm isotopic chain. We can see that the $E_{pair,n}$ vanishes at $A = 144$ and at $A = 162$. It is also approaching zero value at $A = 150$ and at $A = 154$. This is in agreement with the shell-structure behavior shown in Fig. 1(a) by S_{2n} separation energies. Though

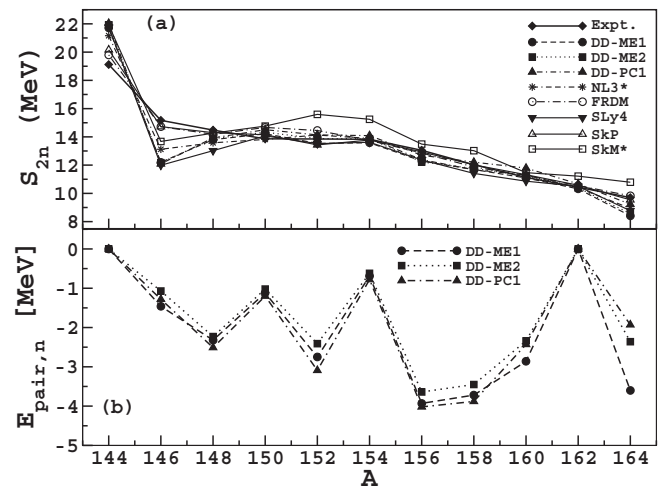


FIG. 1. (a) The two-neutron separation energy S_{2n} , for $^{144-164}\text{Sm}$ nuclei, obtained with DD-ME1, DD-ME2, DD-PC1, and NL3* forces, and compared with the FRDM [149], Skyrme SLy4, SkP, and SkM* forces [146] and with the experimental data [148]. (b) The neutron pairing energy obtained in the CDFT model with DD-ME1, DD-ME2, and DD-PC1 interactions.

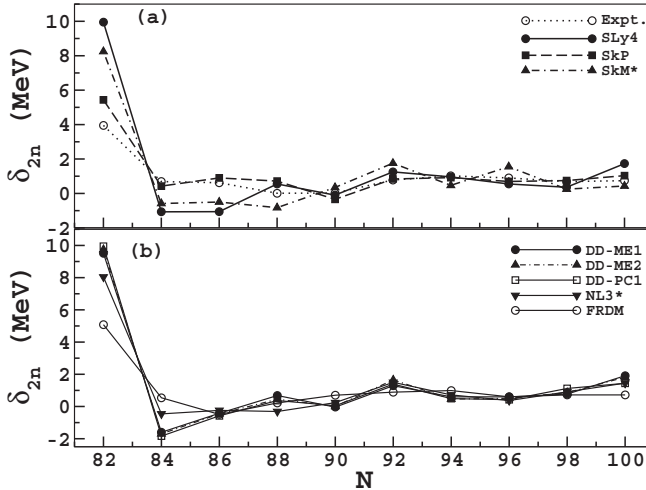


FIG. 2. The two-neutron shell gap δ_{2n} , for $^{144-164}\text{Sm}$ nuclei (a) obtained with Skyrme SLy4, SkP, and SkM* forces [146] and (b) obtained with DD-ME1, DD-ME2, DD-PC1, and NL3* forces, compared with the FRDM [149] and the experimental data [148].

the systematics of S_{2n} separation energies show the neutron shell-closure conspicuously, the vanishing of neutron pairing energy $E_{\text{pair},n}$ at $A = 162$ supports the deformed magic number for $N = 100$.

To confirm the neutron shell closure for $N = 100$, we calculate the two-neutron shell gap $\delta_{2n} = S_{2n}(N, Z) - S_{2n}(N + 2, Z)$, also known as the S_{2n} differential. It is a more sensitive observable for locating the shell closure and is strongly peaked at magic shell closure. The behavior of the S_{2n} differential in Fig. 2 shows exactly the same nature as shown in Fig. 1(a) by two-neutron separation energy (S_{2n}). There are noticeable kinks at $N = 88$ with SLy4, DD-ME1, DD-ME2, and DD-PC1 forces, at $N = 92$ with all the forces, at $N = 96$ with only the SkM* force, and at $N = 100$ with SLy4, DD-ME1, and DD-ME2 forces. Macro-microscopic FRDM calculations and experimental values do not show any kinks except at $N = 82$ ($A = 144$) magic shell closure. The investigations for the magic neutron shell closure, on the basis of the signatures through some sensitive observables, like two-neutron separation energy (S_{2n}) and the S_{2n} differential (δ_{2n}), do not give a completely clear picture. Moreover, zero of the neutron pairing energies ($E_{\text{pair},n}$) indicates the magic shell-closure location. Especially, for the $N = 100$ system, one can notice only a moderate jump in S_{2n} and δ_{2n} behavior with SLy4 and DD-ME forces. This indicates a weaker shell closure which also suggests the model dependence in predicting the shell-closure location.

Table V shows the pairing energy E_{pair} (sum of the neutron and proton contributions) for $^{144-164}\text{Sm}$ calculated by CDFT with effective interactions DD-ME1, DD-ME2, and DD-PC1 and with RMF(NL3*) + BCS formalism. Pairing energy is an important factor which decides the BE, masses of nuclei, etc. For the pairing energy, the data calculated by CDFT more or less agree within the three different density-dependent effective interactions. However, with RMF(NL3*) + BCS formalism the pairing energy is quite different from CDFT.

TABLE V. The pairing energy $-E_{\text{pair}}$ (neutrons + protons) of the ground states of $^{144-164}\text{Sm}$ are calculated with CDFT(DD-ME1, DD-ME2, DD-PC1) and RMF(NL3*) models.

E_{pair} (MeV)	DD-ME1	DD-ME2	DD-PC1	NL3*
^{144}Sm	9.67	9.91	9.90	16.25
^{146}Sm	11.12	10.27	12.61	18.06
^{148}Sm	10.48	10.15	11.71	16.48
^{150}Sm	7.32	6.77	8.67	15.41
^{152}Sm	5.23	4.56	6.45	13.79
^{154}Sm	3.42	2.37	3.90	12.83
^{156}Sm	5.88	5.64	6.80	12.42
^{158}Sm	6.20	6.09	6.98	11.79
^{160}Sm	5.76	5.14	5.66	11.13
^{162}Sm	3.21	3.04	4.61	10.51
^{164}Sm	7.09	5.63	5.73	10.18

We present the rms charge radius (r_{ch}) of Sm isotopes in Table VI. The rms charge radius is calculated from the proton radius by using the relation [154] $r_{\text{ch}} = \sqrt{r_p^2} + 0.64$, taking the finite size of the proton as 0.8 fm. The experimental r_{ch} 's [155] available are given in the table for comparison. Our calculated results show nice agreement with experimental values.

Once we have confirmed that the agreement between our calculations with the experimental r_{ch} is excellent, we have guaranteed that meaningful results will be obtained for the neutron and proton mean-square radii

$$r_{p,n} = \sqrt{\langle r_{p,n}^2 \rangle} \quad (25)$$

by using the same formalism with the same forces.

Having the neutron and proton rms radii [Eq. (25)], the neutron-skin thickness (NST) is usually estimated as their difference:

$$\Delta R = \sqrt{\langle r_n^2 \rangle} - \sqrt{\langle r_p^2 \rangle}. \quad (26)$$

In this way, the NST for Sm isotopes is obtained. In Fig. 3 we compare the root-mean-square radii of proton and neutron,

TABLE VI. The rms charge radius r_{ch} (in fm) for $^{144-164}\text{Sm}$ obtained with CDFT(DD-ME1, DD-ME2, DD-PC1) and RMF(NL3*) models. Available data [155] are included for comparison.

r_{ch} (fm)	EXP [155]	DD-ME1	DD-ME2	DD-PC1	NL3*
^{144}Sm	4.95	4.95	4.95	4.95	4.96
^{146}Sm	4.98	4.98	4.98	4.98	4.98
^{148}Sm	5.00	5.01	5.01	5.05	5.01
^{150}Sm	5.04	5.04	5.04	5.05	5.04
^{152}Sm	5.08	5.09	5.08	5.09	5.09
^{154}Sm	5.10	5.12	5.12	5.12	5.12
^{156}Sm	—	5.14	5.14	5.14	5.14
^{158}Sm	—	5.16	5.16	5.16	5.16
^{160}Sm	—	5.18	5.18	5.18	5.18
^{162}Sm	—	5.20	5.20	5.20	5.20
^{164}Sm	—	5.21	5.21	5.21	5.21

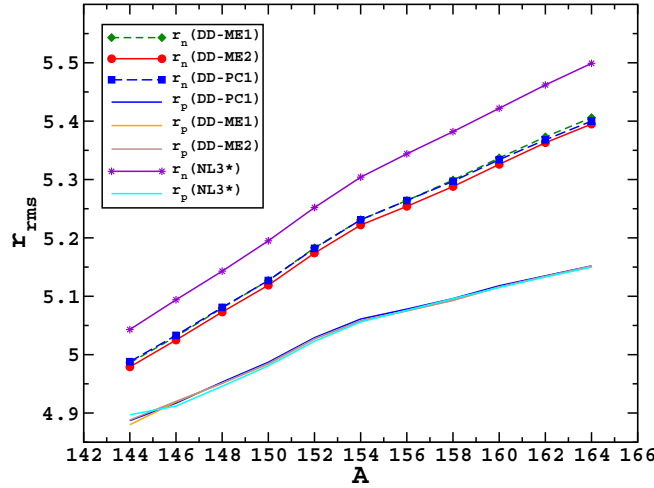


FIG. 3. (Color online) The rms radii r_{rms} for Sm isotopes as a function of mass number A calculated with DD-ME1, DD-ME2, DD-PC1, and NL3* forces.

calculated using CDFT with effective interactions DD-ME and DD-PC and using the constrained axially deformed RMF calculations with effective interaction NL3*. We see that the tendency in rms radii as a function of mass number A is quite similar in both the approaches, but the proton rms radii by both the formalism are almost similar. In general, the neutron rms radii obtained using the density-dependent effective interactions DD-ME and DD-PC are almost equal throughout but, using NL3* it is overestimated by almost a constant factor. We also notice the development of a neutron skin as evidenced by the large difference between the neutron and proton rms radii.

This is clearly seen in Fig. 4, where we plot the difference between the rms radii of neutrons and protons [Eq. (26)]. The latter is a simple measure of a neutron (proton) skin emergence in Sm isotopes from the considered isotopic chain. We can see from Fig. 4 that ΔR increases monotonically with neutron

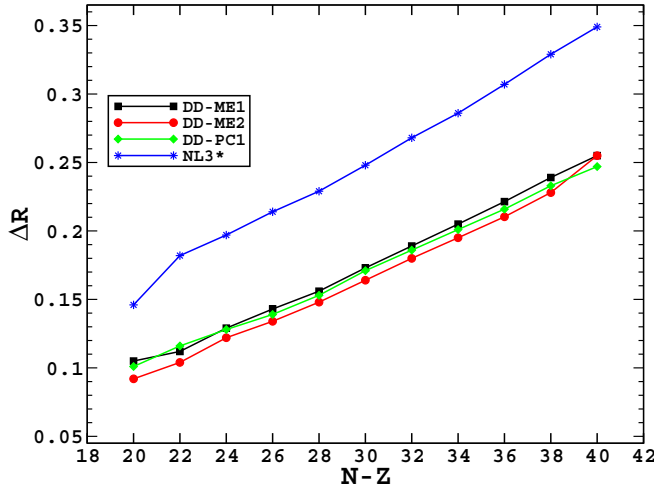


FIG. 4. (Color online) The NST ΔR for Sm isotopes as a function of mass number A calculated with DD-ME1, DD-ME2, DD-PC1, and NL3* forces.

excess in the chain of Sm isotopes. The constrained axially deformed RMF with BCS pairing results for the different ΔR systematically overestimate the CDFT results. The behavior of the NST displayed in Fig. 4 can be understood in terms of the slope parameter of the symmetry energy at saturated density L [156]. It has been predicted that the NST calculated with the successful EDFs including Skyrme, Gogny, and RMF models is linearly correlated with L . It has also been shown that the slope parameter of the symmetry energy at saturation density L is larger with the RMF (NL3*) model than that found by CDFT calculations with DD-ME1, DD-ME2, and DD-PC1 interactions [156]. This supports the neutron rms radius and the NST behavior, as shown in Fig. 3 and Fig. 4, respectively.

C. Quadrupole deformation parameter

We have predicted the quadrupole deformations of Sm isotopes with the various models considered here. Our calculated values are compared with the systematic calculations in the macro-microscopic FRDM [157], and the predictions within the HFB + THO + LN + PNP method based on the Skyrme SLy4, SkP, and SkM* interactions [146], as well as with the available experimental data [158]. Table VII contains the systematics in deformation properties calculated with different models and is also consistent with the known experimental trend, except in the case of FRDM [157] results. The spherical shapes in $^{144,146}\text{Sm}$ and the weakly deformed ^{148}Sm are well reproduced. The deformations in $^{150-164}\text{Sm}$ show good agreement with available experimental data [158]. Noticeably, the quadrupole deformation values for higher mass nuclei show an almost constant nature in the case of different model calculations.

D. Potential energy surface

We have performed the PES calculations for even-even $^{144-164}\text{Sm}$ using CDFT with density-dependent effective interactions DD-ME1, DD-ME2, and DD-PC1 (point-coupling) and with a constrained axially deformed RMF model with effective interaction NL3*. These potential energy curves for $^{144-164}\text{Sm}$ obtained with effective interactions DD-ME1, DD-ME2, DD-PC1, and NL3* are shown in Figs. 5, 6, 7, and 8, respectively. Similar patterns are found for all the effective interactions. The ground state of ^{144}Sm is found to be spherical and has about a 13-MeV stiff barrier against deformation. The ground state of ^{146}Sm is still spherical; its barrier becomes lower and is around 9 MeV against the deformation. With the increase of the neutron number, the ground state gradually moves towards the deformed side and the potential energy curve becomes softer. Finally, well-deformed $^{154-164}\text{Sm}$ is reproduced. To analyze the transition region of shape change of the Sm isotopes with the neutron number, we have calculated the differences ΔE of the ground-state BE with the binding energy of the spherical shape of Sm isotopes. This is presented in Table VIII with different effective interactions DD-ME1, DD-ME2, DD-PC1, and NL3*.

These differences will tell us the softness of Sm isotopes against the deformation and may give us a hint on the phase transition of the nuclear shape. We can see from Table VIII that

TABLE VII. The quadrupole deformation parameter β_2 of the ground states of $^{144-164}\text{Sm}$ calculated with DD-ME1, DD-ME2, DD-PC1, and NL3* forces. Comparison with FRDM [157], Skyrme SLy4, SkP, and SkM* forces [146], and the experimental data [158], wherever available, are presented.

β_2	EXP	DD-ME1	DD-ME2	DD-PC1	NL3*	FRDM	SLy4	SkP	SkM*
^{144}Sm	0.09	-0.00	-0.00	-0.00	-0.00	0.000	0.000	0.000	0.000
^{146}Sm	—	-0.08	-0.08	-0.07	0.00	0.000	0.046	0.056	0.071
^{148}Sm	0.14	0.15	0.15	0.16	0.13	0.161	0.157	0.140	0.175
^{150}Sm	0.19	0.21	0.22	0.22	0.20	0.206	0.219	0.204	0.247
^{152}Sm	0.31	0.29	0.29	0.29	0.28	0.243	0.290	0.292	0.298
^{154}Sm	0.34	0.33	0.33	0.33	0.32	0.270	0.317	0.318	0.321
^{156}Sm	—	0.33	0.33	0.33	0.34	0.279	0.326	0.328	0.334
^{158}Sm	—	0.34	0.34	0.34	0.35	0.279	0.334	0.333	0.342
^{160}Sm	—	0.36	0.36	0.36	0.36	0.290	0.338	0.337	0.344
^{162}Sm	—	0.36	0.36	0.36	0.36	0.300	0.339	0.340	0.344
^{164}Sm	—	0.36	0.37	0.36	0.37	0.302	0.338	0.344	0.345

from $^{144-164}\text{Sm}$, the energy differences between the ground state and the state with spherical shape change from 0 MeV to maximum 17 MeV within all the effective interactions. There are two jumps in the energy difference. The first jump appears at ^{148}Sm and the second at ^{154}Sm , which suggests the shape change from spherical to critical-point nuclei and finally to axially deformed nuclei. The potential energy curves for ^{148}Sm , ^{150}Sm , and ^{152}Sm are relatively flat; i.e., they are β_2 -soft nuclei in the transition region between spherical and axially symmetric deformed nuclei. The present PES studies are found to be in good agreement with earlier study done by Meng *et al.* [159] using a constrained RMF model with NL1, NL3, NLSH, and TM1 effective interactions. It can also be noticed that the PES curve of ^{164}Sm is flat and the fact that there is a discontinuity in ΔE at ^{162}Sm compared to its neighbors supports the magic structure as reported with RMF formalism [53,54]. In addition to this, it is worth mentioning that the RMF calculation of shell energy, two-neutron separation energy, two-neutron differential [53], and the local energy η in the infinite nuclear matter (INM)

mass model [150] predict $N = 100$ as a deformed magic number for ^{162}Sm . Also, the dominant β^- -decay mode of the neutron-rich ^{162}Sm shows the extra stability as reported by Asai *et al.* [151]. It is worth mentioning that the results of self-consistent HFB calculations based on the D1S [143] Gogny [144] effective nucleon-nucleon interaction show a very similar structure by other isotopic chains between $Z = 50-62$ and $N = 60-100$ [53,54]. Further, for PES study done using the Gogny interaction with the D1S parametrization, a general behavior has been found along different regions of the periodic table that, as the neutron number increases above $N = 100$, the quadrupole deformation decreases gradually and becomes slightly negative as one approaches the neutron drip line [145,160-162]. Because of the magic properties of $N = 100$, this isotope will serve as a waiting point in the nucleosynthesis of the rapid neutron capture process (r process) [163]. This prediction has an important consequence in the formation of heavy nuclei in astrophysical objects.

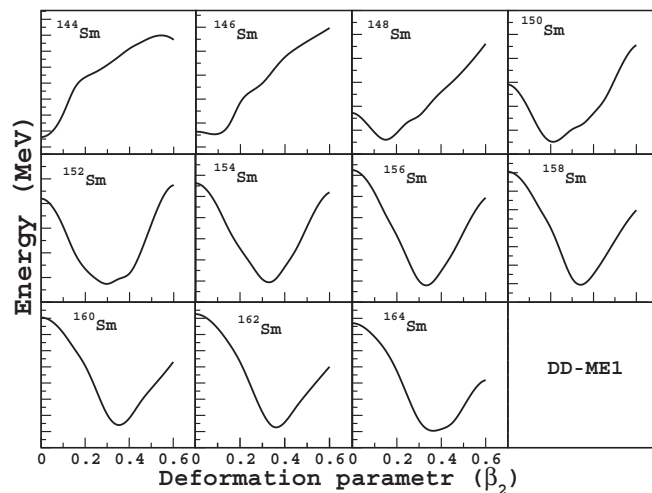


FIG. 5. The potential energy curves for $^{144-164}\text{Sm}$ obtained with the density-dependent DD-ME1 parametrization.

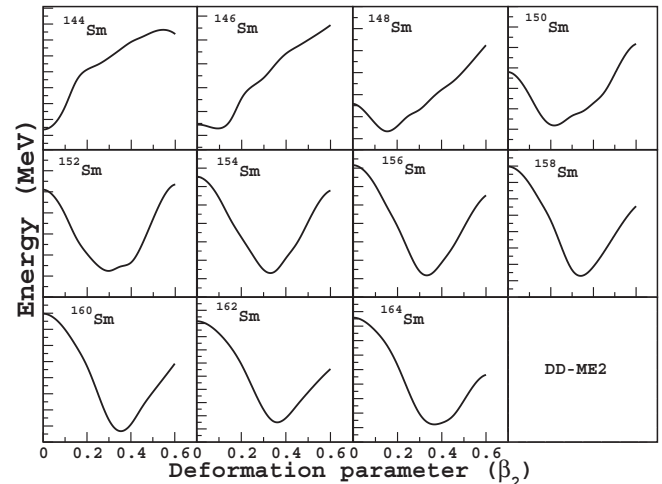


FIG. 6. The potential energy curves for $^{144-164}\text{Sm}$ obtained with the density-dependent DD-ME2 parametrizations.

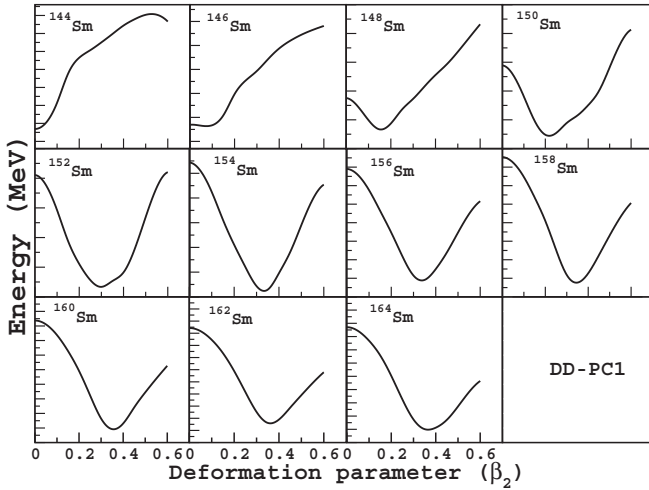


FIG. 7. The potential energy curves for $^{144-164}\text{Sm}$ obtained with the density-dependent DD-PC1 (point-coupling) parametrizations.

E. Ground-state single-particle levels

A detailed study of single-particle levels are one of the important aspects when discussing nuclear structure and understanding the physical origin for the critical-point nuclei. In Fig. 9 we plot the single-neutron levels for $^{144-164}\text{Sm}$ nuclei lying between -20 and 0 MeV. The figure presents results calculated with the most recent well-established effective interaction DD-ME2. The other interactions give similar structure and thus are not presented here. From Fig. 9 one finds that, as the neutron number changes throughout the Sm isotopic chain, the single-neutron levels and hence the structure of Fermi surfaces of these nuclei show variations. Even and odd parity levels are represented by black and red, respectively. The Fermi level is presented here by a dashed line. In general, from Fig. 9 one finds a consistency between the shell-structure evolution and the shape evolution in Sm isotopes with increasing neutron number. From the figure we

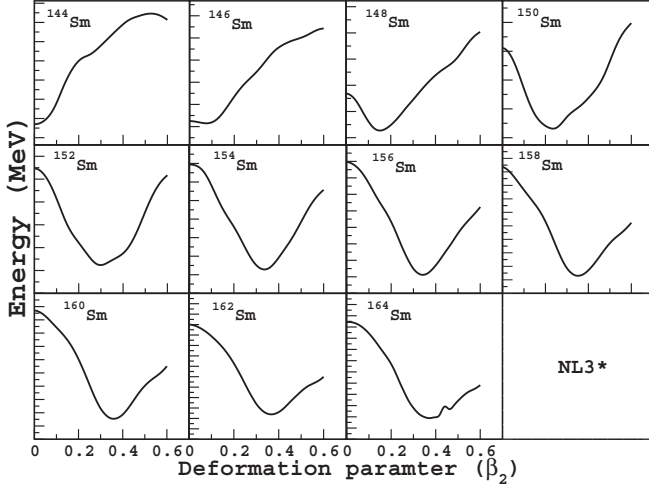


FIG. 8. The potential energy curves for $^{144-164}\text{Sm}$ obtained with the NL3* parametrizations.

TABLE VIII. The difference of the total BE ΔE between the spherical state and the ground state in units of MeV calculated with DD-ME1, DD-ME2, DD-PC1, and NL3* forces.

ΔE	DD-ME1	DD-ME2	DD-PC1	NL3*
^{144}Sm	0.00	0.00	0.00	0.00
^{146}Sm	0.21	0.31	0.11	0.20
^{148}Sm	2.24	2.51	2.18	2.82
^{150}Sm	4.78	5.23	4.89	5.58
^{152}Sm	6.91	7.71	7.54	8.46
^{154}Sm	9.38	10.46	10.39	11.32
^{156}Sm	10.90	11.96	12.04	13.70
^{158}Sm	12.22	13.35	13.55	16.13
^{160}Sm	13.30	14.59	14.92	16.34
^{162}Sm	14.01	15.35	15.69	17.24
^{164}Sm	13.31	14.73	15.46	17.10

see the shape transitions in Sm isotopes. For ^{144}Sm spherical symmetry is better restored with large single-neutron gap in the neutron Fermi surface. With the increasing neutron number the deformation develops. The deformation in ^{146}Sm is still small and the energy gap can be clearly seen from the single-particle spectra. The critical-point nuclei $^{148-152}\text{Sm}$ belong to a transition area in which the energy gap still exists, but are much smaller than that in $^{144,146}\text{Sm}$. In general, we can say that the Fermi level slowly increases. A good deformation seems to be reached at $A = 148$ or $A = 150$ with a rather constant level density, from that moment the Fermi levels stays roughly constant up to ^{162}Sm . These characteristics in microscopic shell structure can be viewed as the signature of the critical-point symmetry. The large shell gap in the neutron Fermi surface in the case of ^{162}Sm indicates the properties of a magic nuclei, supporting the earlier reported results [52,53,150,151].

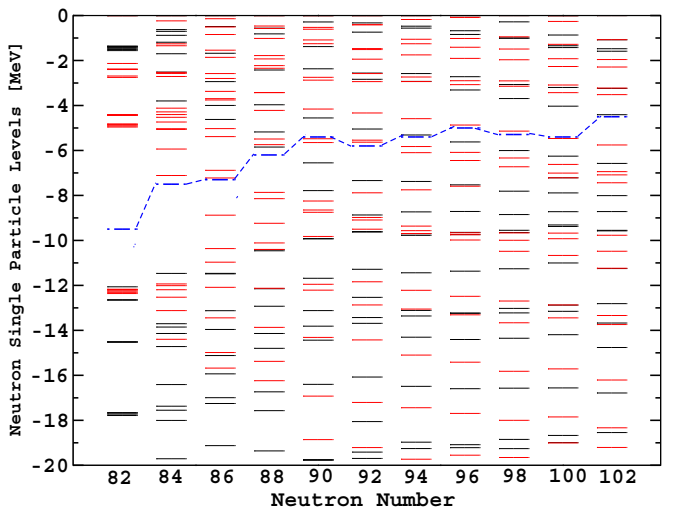


FIG. 9. (Color online) The single-neutron levels for even-even $^{144-164}\text{Sm}$ nuclei obtained with the density-dependent DD-ME2 parametrizations.

IV. CONCLUSION

In this work, we have carried out systematic investigations to study the bulk properties and the microscopic structure of neutron-rich, even-even $^{144-164}\text{Sm}$ transitional nuclei. The investigations have been done within CDFT, and the explicit density-dependent effective interactions as DD-M1, DD-ME2, and DD-PC1 (point coupling) were used in the calculations. We have also carried out these investigations using the constrained axially deformed RMF model with NL3* parametrization. Proper treatment of the pairing correlations is given in both formalisms. We have calculated the BE, two-neutron separation energy (S_{2n}), two-neutron shell gap (δ_{2n}), neutron pairing energy ($E_{\text{pair},n}$), rms radii, NST, and quadrupole deformation parameter to understand the ground-state properties of these nuclei. The potential energy surface and the single-particle levels have been studied to understand the phase transition and the critical-point behavior of these nuclei. Present calculations have also been compared with the self-consistent HFB + THO + LN + PNP method based on the Skyrme SLy4, SkP, and SkM* interactions, macro-microscopic FRDM, as well as on the experimental data, wherever available.

In summary, the microscopic investigations are done to understand the shape evolution from spherical to the axially deformed shapes in even-even Sm isotopes and to investigate the deformed magic number for $N = 100$ as reported by the authors of Refs. [52,53,150,151]. The bulk properties

are quite well reproduced in our calculations using different effective interactions and are in good agreement within the different model interactions, as well as with the experimental data. ^{148}Sm , ^{150}Sm , and ^{152}Sm are found to be soft against the β deformation in their corresponding potential energy curves. We analyze the ground-state single-particle spectra and find that the single-particle levels in ^{148}Sm , ^{150}Sm , and ^{152}Sm distribute more uniformly. Different sensitive observables like two-neutron separation energy (S_{2n}), two-neutron shell gap (δ_{2n}), neutron pairing energy ($E_{\text{pair},n}$), total BE difference (ΔE), and single-particle level scheme are investigated to identify the shell-closure location at $N = 100$. Except for vanishing of the neutron paring energy $E_{\text{pair},n}$ at $A = 162$, other signatures are not very evident, indicating a weaker shell closure at $N = 100$. The investigations also suggest the model dependence on predicting the shell-closure location. However, the experimental confirmation of the shell-closure properties of ^{162}Sm is still awaiting. Overall, good agreement is found between the calculated and experimental results, wherever available.

ACKNOWLEDGMENTS

We are very grateful to T. Nikšić, N. Paar, D. Vretenar, and P. Ring for making available the DIRHB package of FORTRAN computer codes. A. Karim would like to pay his Special thanks to T. Nikšić and A. V. Afanasjev for their help in understanding and running the DIRHB package and to Professor P. Ring for helpful discussions and useful comments through email.

-
- [1] A. Bohr, Mat. Fys. Medd. - K. Danske Vidensk. Selsk. **26**(14) (1952).
 - [2] L. Wilets and M. Jean, *Phys. Rev.* **102**, 788 (1956).
 - [3] A. S. Davydov and G. F. Filippov, *Nucl. Phys.* **8**, 237 (1958).
 - [4] A. S. Davydov and A. A. Chaban, *Nucl. Phys.* **20**, 499 (1960).
 - [5] G. Gneuss, U. Mosel, and W. Greiner, *Phys. Lett. B* **30**, 397 (1969).
 - [6] F. Iachello, in *Group Theoretical Methods in Physics*, edited by A. Böhm *et al.*, Lecture Notes in Physics Vol. 90 (Springer, Berlin, 1979), p. 240; *Symmetries in Particle Physics*, edited by A. Chodos and C. Tze (Plenum, New York, 1984), p. 47.
 - [7] J. M. Arias, *Phys. Rev. C* **63**, 034308 (2001).
 - [8] J. Y. Zhang, N. V. Zamfir, R. F. Casten, and M. A. Caprio, *Phys. Rev. C* **64**, 017302 (2001).
 - [9] J. Jolie, R. F. Casten, P. von Brentano, and V. Werner, *Phys. Rev. Lett.* **87**, 162501 (2001).
 - [10] A. Frank, C. E. Alonso, and J. M. Arias, *Phys. Rev. C* **65**, 014301 (2001).
 - [11] M. A. Caprio, *Phys. Rev. C* **65**, 031304 (2002).
 - [12] N. V. Zamfir, P. von Brentano, R. F. Casten, and J. Jolie, *Phys. Rev. C* **66**, 021304(R) (2002).
 - [13] V. Werner, P. von Brentano, R. F. Casten, and J. Jolie, *Phys. Lett. B* **527**, 55 (2002).
 - [14] J. Jolie, P. Cejnar, R. F. Casten, S. Heinze, A. Linnemann, and V. Werner, *Phys. Rev. Lett.* **89**, 182502 (2002).
 - [15] R. M. Clark, M. Cromaz, M. A. Deleplanque, R. M. Diamond, P. Fallon, A. Gorgen, I. Y. Lee, A. O. Macchiavelli, F. Stephens, and D. Ward, *Phys. Rev. C* **67**, 041302(R) (2003).
 - [16] A. Levitan and J. N. Ginocchio, *Phys. Rev. Lett.* **90**, 212501 (2003).
 - [17] L. Fortunato and A. Vitturi, *J. Phys. G* **29**, 1341 (2003).
 - [18] F. Iachello and A. Arima, *The Interacting Boson Model* (Cambridge University Press, Cambridge, UK, 1987).
 - [19] A. E. L. Dieperink, O. Scholten, and F. Iachello, *Phys. Rev. Lett.* **44**, 1747 (1980).
 - [20] D. H. Feng, R. Gilmore, and S. R. Deans, *Phys. Rev. C* **23**, 1254 (1981).
 - [21] F. Iachello, N. V. Zamfir, and R. F. Casten, *Phys. Rev. Lett.* **81**, 1191 (1998).
 - [22] F. Iachello, *Phys. Rev. Lett.* **85**, 3580 (2000).
 - [23] F. Iachello, *Phys. Rev. Lett.* **87**, 052502 (2001).
 - [24] R. F. Casten and N. V. Zamfir, *Phys. Rev. Lett.* **87**, 052503 (2001).
 - [25] R. F. Casten, M. Wilhelm, E. Radermacher, N. V. Zamfir, and P. von Brentano, *Phys. Rev. C* **57**, R1553(R) (1998).
 - [26] N. V. Zamfir, R. F. Casten, M. A. Caprio, C. W. Beausang, R. Krucken, J. R. Novak, J. R. Cooper, G. Cata-Danil, and C. J. Barton, *Phys. Rev. C* **60**, 054312 (1999).
 - [27] T. Klug, A. Dewald, V. Werner, P. von Brentano, and R. F. Casten, *Phys. Lett. B* **495**, 55 (2000).
 - [28] R. F. Casten, D. Kusnezov, and N. V. Zamfir, *Phys. Rev. Lett.* **82**, 5000 (1999).

- [29] R. Krucken *et al.*, *Phys. Rev. Lett.* **88**, 232501 (2002).
- [30] M. A. Caprio *et al.*, *Phys. Rev. C* **66**, 054310 (2002).
- [31] P. G. Bizzeti and A. M. Bizzeti-Sona, *Phys. Rev. C* **66**, 031301(R) (2002).
- [32] C. Hutter *et al.*, *Phys. Rev. C* **67**, 054315 (2003).
- [33] R. M. Clark *et al.*, *Phys. Rev. C* **68**, 037301 (2003).
- [34] R. Bijker, R. F. Casten, N. V. Zamfir, and E. A. McCutchan, *Phys. Rev. C* **68**, 064304 (2003).
- [35] C. Fransen, N. Pietralla, A. Linnemann, V. Werner, and R. Bijker, *Phys. Rev. C* **69**, 014313 (2004).
- [36] D. Tonev, A. Dewald, T. Klug, P. Petkov, J. Jolie, A. Fitzler, O. Moller, S. Heinze, P. von Brentano, and R. F. Casten, *Phys. Rev. C* **69**, 034334 (2004).
- [37] R. Bijker, R. F. Casten, N. V. Zamfir, and E. A. McCutchan, *Phys. Rev. C* **69**, 059901(E) (2004).
- [38] M. A. Caprio, *Phys. Rev. C* **69**, 044307 (2004).
- [39] D. Bonatsos, D. Lenis, N. Minkov, D. Petrellis, P. P. Raychev, and P. A. Terziev, *Phys. Rev. C* **70**, 024305 (2004).
- [40] N. Pietralla and O. M. Gorbachenko, *Phys. Rev. C* **70**, 011304(R) (2004).
- [41] P. G. Bizzeti and A. M. Bizzeti-Sona, *Eur. Phys. J. A* **20**, 179 (2004); *Phys. Rev. C* **70**, 064319 (2004).
- [42] E. Padilla-Rodal *et al.*, *Phys. Rev. Lett.* **94**, 122501 (2005).
- [43] J. A. Winger *et al.*, *Phys. Rev. C* **81**, 044303 (2010).
- [44] H. Iwasaki *et al.*, *Eur. Phys. J. A* **25**, 415 (2005).
- [45] M. Honma, T. Otsuka, T. Mizusaki, and M. Hjorth-Jensen, *Phys. Rev. C* **80**, 064323 (2009).
- [46] M. Bender, G. F. Bertsch, and P. H. Heenen, *Phys. Rev. C* **78**, 054312 (2008).
- [47] R. V. F. Janssens, *Nature (London)* **459**, 1069 (2009).
- [48] A. Ozawa, T. Kobayashi, T. Suzuki, K. Yoshida, and I. Tanihata, *Phys. Rev. Lett.* **84**, 5493 (2000).
- [49] O. Sorlina and M. G. Porquet, *Prog. Part. Nucl. Phys.* **61**, 602 (2008).
- [50] M. Brack *et al.*, *Rev. Mod. Phys.* **44**, 320 (1972).
- [51] J. H. Hamilton *et al.*, *J. Phys. G* **10**, L87 (1984).
- [52] J. H. Hamilton, *Progress in Particle and Nuclear Physics*, edited by A. Faessler (Pergamon Press, New York, 1985), Vol. 15, p. 107.
- [53] L. Satpathy and S. K. Patra, *J. Phys. G* **30**, 771 (2004).
- [54] L. Satpathy and S. K. Patra, *Nucl. Phys. A* **722**, C24 (2003).
- [55] L. S. Danu *et al.*, *Phys. Rev. C* **81**, 014311 (2010).
- [56] R. J. Furnstahl and B. D. Serot, *Nucl. Phys. A* **673**, 298 (2000).
- [57] G. Lalazissis, P. Ring, and D. Vretenar (editors), *Extended Density Functionals in Nuclear Structure Physics*, Springer Lecture Notes in Physics Vol. 641 (Springer, Berlin, 2004).
- [58] R. J. Furnstahl, in *Renormalization Group and Effective Field Theory Approaches to Many-Body Systems*, Proceedings of the ECT School, Springer Lecture Notes in Physics Vol. 852 (Springer, Berlin, 2012), p. 133.
- [59] R. J. Furnstahl, G. Rupak, and T. Schäfer, *Annu. Rev. Nucl. Part. Sci.* **58**, 1 (2008).
- [60] B. B. Serot and J. D. Walecka, *Advances of Nuclear Physics*, edited by J. W. Negele and E. Vogt (Plenum, New York, 1986), Vol. 16.
- [61] P. Ring, *Prog. Part. Nucl. Phys.* **37**, 193 (1996).
- [62] J. Meng and P. Ring, *Phys. Rev. Lett.* **77**, 3963 (1996).
- [63] J. Meng, *Nucl. Phys. A* **635**, 3 (1998).
- [64] J. Meng and P. Ring, *Phys. Rev. Lett.* **80**, 460 (1998).
- [65] J. N. Ginocchio, *Phys. Rev. Lett.* **78**, 436 (1997).
- [66] J. Meng, K. Sugawara-Tanabe, S. Yamaji, P. Ring, and A. Arima, *Phys. Rev. C* **58**, R628 (1998).
- [67] J. Meng, K. Sugawara-Tanabe, S. Yamaji, and A. Arima, *Phys. Rev. C* **59**, 154 (1999).
- [68] J. N. Ginocchio, *Phys. Rep.* **315**, 231 (1999).
- [69] S. G. Zhou, J. Meng, and P. Ring, *Phys. Rev. Lett.* **91**, 262501 (2003).
- [70] B. D. Serot and J. D. Walecka, *Int. J. Mod. Phys. E* **6**, 515 (1997).
- [71] M. Bender, P.-H. Heenen, and P.-G. Reinhard, *Rev. Mod. Phys.* **75**, 121 (2003).
- [72] D. Vretenar, A. V. Afanasjev, G. A. Lalazissis, and P. Ring, *Phys. Rep.* **409**, 101 (2005).
- [73] B. G. Carlsson, J. Dobaczewski, and M. Kortelainen, *Phys. Rev. C* **78**, 044326 (2008).
- [74] W. Kohn and L. J. Sham, *Phys. Rev.* **137**, A1697 (1965).
- [75] W. Kohn and L. J. Sham, *Phys. Rev.* **140**, A1133 (1965).
- [76] A. Sobczewski and K. Pomorski, *Prog. Part. Nucl. Phys.* **58**, 292 (2007).
- [77] T. D. Cohen, R. J. Furnstahl, and D. K. Griegel, *Phys. Rev. C* **45**, 1881 (1992).
- [78] W. Koepf and P. Ring, *Nucl. Phys. A* **493**, 61 (1989).
- [79] W. Koepf and P. Ring, *Nucl. Phys. A* **511**, 279 (1990).
- [80] A. V. Afanasjev and H. Abusara, *Phys. Rev. C* **81**, 014309 (2010).
- [81] U. Hofmann and P. Ring, *Phys. Lett. B* **214**, 307 (1988).
- [82] A. V. Afanasjev and P. Ring, *Phys. Rev. C* **62**, 031302(R) (2000).
- [83] A. V. Afanasjev and H. Abusara, *Phys. Rev. C* **82**, 034329 (2010).
- [84] J. Dobaczewski and J. Dudek, *Phys. Rev. C* **52**, 1827 (1995).
- [85] U. Post, E. Wüst, and U. Mosel, *Nucl. Phys. A* **437**, 274 (1985).
- [86] J. König and P. Ring, *Phys. Rev. Lett.* **71**, 3079 (1993).
- [87] H. Zduńczuk, W. Satula, and R. A. Wyss, *Phys. Rev. C* **71**, 024305 (2005).
- [88] A. V. Afanasjev, *Phys. Rev. C* **78**, 054303 (2008).
- [89] Y. M. Engel, D. M. Brink, K. Geoke, S. J. Krieger, and D. Vauterin, *Nucl. Phys. A* **249**, 215 (1975).
- [90] V. O. Nesterenko, W. Kleinig, J. Kvasil, P. Vesely, and P.-G. Reinhard, *Int. J. Mod. Phys. E* **17**, 89 (2008).
- [91] N. Hinohara, T. Nakatsukasa, M. Matsuo, and K. Matsuyanagi, *Prog. Theor. Phys.* **115**, 567 (2006).
- [92] A. S. Umar and V. E. Oberacker, *Phys. Rev. C* **73**, 054607 (2006).
- [93] M. Bender, J. Dobaczewski, J. Engel, and W. Nazarewicz, *Phys. Rev. C* **65**, 054322 (2002).
- [94] W. Satula, in *Nuclear Structure 98*, edited by C. Baktash, AIP Conference Proceeding No. 481 (AIP, New York, 1999), p. 114.
- [95] T. Duguet, P. Bonche, P.-H. Heenen, and J. Meyer, *Phys. Rev. C* **65**, 014310 (2001).
- [96] A. V. Afanasjev, T. L. Khoo, S. Frauendorf, G. A. Lalazissis, and I. Ahmad, *Phys. Rev. C* **67**, 024309 (2003).
- [97] M. Matev, A. V. Afanasjev, J. Dobaczewski, G. A. Lalazissis, and W. Nazarewicz, *Phys. Rev. C* **76**, 034304 (2007).
- [98] J. Dobaczewski, J. Dudek, and R. Wyss, *Phys. Rev. C* **67**, 034308 (2003).
- [99] K. Rutz, M. Bender, P.-G. Reinhard, and J. A. Maruhn, *Phys. Lett. B* **468**, 1 (1999).
- [100] T. Nikšić, D. Vretenar, P. Finelli, and P. Ring, *Phys. Rev. C* **66**, 024306 (2002).

- [101] G. A. Lalazissis, T. Nikšić, D. Vretenar, and P. Ring, *Phys. Rev. C* **71**, 024312 (2005).
- [102] T. Nikšić, D. Vretenar, and P. Ring, *Phys. Rev. C* **78**, 034318 (2008).
- [103] X. Roca-Maza, X. Viñas, M. Centelles, P. Ring, and P. Schuck, *Phys. Rev. C* **84**, 054309 (2011).
- [104] N. Paar, D. Vretenar, E. Khan, and G. Coló, *Rep. Prog. Phys.* **70**, 691 (2007).
- [105] T. Nikšić, D. Vretenar, and P. Ring, *Prog. Part. Nucl. Phys.* **66**, 519 (2011).
- [106] H. Abusara, A. V. Afanasjev, and P. Ring, *Phys. Rev. C* **85**, 024314 (2012).
- [107] A. Makishima, M. Adachi, H. Taketani, and M. Ishii, *Phys. Rev. C* **34**, 576 (1986).
- [108] E. Veje *et al.*, *Nucl. Phys. A* **109**, 489 (1968).
- [109] P. Regan, G. D. Dracoulis, A. P. Byrne, G. J. Lane, T. Kibedi, P. M. Walker, and A. M. Bruce, *Phys. Rev. C* **51**, 1745 (1995).
- [110] W. Starzecki *et al.*, *Phys. Lett. B* **200**, 419 (1988).
- [111] A. M. Bruce, P. M. Walker, P. H. Regan, G. D. Dracoulis, A. P. Byrne, T. Kibedi, G. J. Lane, and K. C. Yeung, *Phys. Rev. C* **50**, 480 (1994).
- [112] J. D. Walecka, *Ann. Phys. (NY)* **83**, 491 (1974).
- [113] J. Boguta and A. R. Bodmer, *Nucl. Phys. A* **292**, 413 (1977).
- [114] W. Pannert, P. Ring, and J. Boguta, *Phys. Rev. Lett.* **59**, 2420 (1987).
- [115] Y. K. Gambhir, P. Ring, and A. Thimet, *Ann. Phys. (NY)* **198**, 132 (1990).
- [116] G. A. Lalazissis, S. Karatzikos, R. Fission, D. Peña Arteaga, A. V. Afanasjev, and P. Ring, *Phys. Lett. B* **671**, 36 (2009).
- [117] T. Nikšić, N. Paar, D. Vretenar, and P. Ring, *Comp. Phys. Commun.* **185**, 1808 (2014).
- [118] S. Typel and H. H. Wolter, *Nucl. Phys. A* **656**, 331 (1999).
- [119] P. G. Reinhard, M. Rufa, J. Maruhn, W. Greiner, and J. Friedrich, *Z. Phys. A-Atomic Nuclei* **323**, 13 (1986).
- [120] G. A. Lalazissis, J. König, P. Ring, *Phys. Rev. C* **55**, 540 (1997).
- [121] B. G. Todd-Rutel and J. Piekarewicz, *Phys. Rev. Lett.* **95**, 122501 (2005).
- [122] R. Brockmann and H. Toki, *Phys. Rev. Lett.* **68**, 3408 (1992).
- [123] F. Hofmann, C. M. Keil, and H. Lenske, *Phys. Rev. C* **64**, 034314 (2001).
- [124] F. de Jong and H. Lenske, *Phys. Rev. C* **57**, 3099 (1998).
- [125] G. Audi, A. H. Wapstra, and C. Thibault, *Nucl. Phys. A* **729**, 337 (2003).
- [126] A. Krasznauskay *et al.*, *Phys. Rev. Lett.* **82**, 3216 (1999).
- [127] E. G. Nadjkov, K. P. Marinova, and Yu. P. Gangrsky, *At. Data Nucl. Data Tables* **56**, 133 (1994).
- [128] P. Manakos and T. Mannel, *Z. Phys. A-Atomic Nuclei* **330**, 223 (1988).
- [129] J. J. Rusnak and R. J. Furnstahl, *Nucl. Phys. A* **627**, 495 (1997).
- [130] T. Bürenich, D. G. Madland, J. A. Maruhn, and P. G. Reinhard, *Phys. Rev. C* **65**, 044308 (2002).
- [131] P. W. Zhao, Z. P. Li, J. M. Yao, and J. Meng, *Phys. Rev. C* **82**, 054319 (2010).
- [132] B. A. Nikolaus, T. Hoch, and D. G. Madland, *Phys. Rev. C* **46**, 1757 (1992).
- [133] P. Ring and P. Schuck, *The Nuclear Many-Body Problem* (Springer-Verlag, Berlin, 1980).
- [134] A. Staszack, M. Stoitsov, A. Baran, and W. Nazarewicz, *Eur. Phys. J. A* **46**, 85 (2010).
- [135] T. Gonzales-Llarena, J. L. Egido, G. A. Lalazissis, and P. Ring, *Phys. Lett. B* **379**, 13 (1996).
- [136] J. Meng, H. Toki, S.-G. Zhou, S.-Q. Zhang, W.-H. Long, and L.-S. Geng, *Prog. Part. Nucl. Phys.* **57**, 470 (2006).
- [137] G. A. Lalazissis, D. Vretenar, P. Ring, M. Stoitsov, and L. M. Robledo, *Phys. Rev. C* **60**, 014310 (1999).
- [138] G. A. Lalazissis, D. Vretenar, and P. Ring, *Nucl. Phys. A* **650**, 133 (1999).
- [139] J. Dobaczewski, H. Flocard, and J. Treiner, *Nucl. Phys. A* **422**, 103 (1984).
- [140] S. K. Patra, *Phys. Rev. C* **48**, 1449 (1993).
- [141] M. A. Preston and R. K. Bhaduri, *Structure of Nucleus* (Addison-Wesley, Boston, 1982), Chap. 8, p. 309.
- [142] D. G. Madland and J. R. Nix, *Nucl. Phys. A* **476**, 1 (1981); P. Möller and J. R. Nix, *At. Data and Nucl. Data Tables* **39**, 213 (1988).
- [143] J. Dechargé, D. Gogny, *Phys. Rev. C* **21**, 1568 (1980).
- [144] J. F. Berger, M. Girod, and D. Gogny, *Nucl. Phys. A* **428**, 23c (1984).
- [145] M. V. Stoitsov, J. Dobaczewski, W. Nazarewicz, S. Pittel, and D. J. Dean, *Phys. Rev. C* **68**, 054312 (2003).
- [146] see <http://www.fuw.edu.pl/~dobaczew/thodri/thodri.html>
- [147] G. Audi, O. Bersillon, and J. Blachot, *Nucl. Phys. A* **624**, 1 (1997).
- [148] www.nndc.bnl.gov
- [149] P. Möller, J. R. Nix, and K.-L. Kratz, *At. Data Nucl. Data Tables* **66**, 131 (1997).
- [150] R. C. Nayak and L. Satpathy, *At. Data Nucl. Data Tables* **73**, 213 (1999).
- [151] M. Asai *et al.*, Jaeri Tandem Annu. Rep. No. **2000**, 13 (2001).
- [152] M. Del Estal, M. Centelles, X. Viñas, and S. K. Patra, *Phys. Rev. C* **63**, 044321 (2001).
- [153] Tapas Sil, S. K. Patra, B. K. Sharma, M. Centelles, and X. Viñas, *Phys. Rev. C* **69**, 044315 (2004).
- [154] S. K. Patra and C. R. Praharaj, *Phys. Rev. C* **44**, 2552 (1991).
- [155] I. Angeli, *At. Data Nucl. Data Tables* **99**, 69 (2013).
- [156] X. Viñas, M. Centelles, X. Roca-Maza, and M. Warda, *Eur. Phys. J. A* **50**, 27 (2014).
- [157] P. Möller *et al.*, *At. Data Nucl. Data Tables* **59**, 185 (1995).
- [158] S. Raman *et al.*, *At. Data Nucl. Data Tables* **78**, 1 (2001).
- [159] J. Meng, W. Zhang, S. G. Zhou, H. Toki, and L. Geng, *Eur. Phys. J. A* **25**, 23 (2005).
- [160] See www-phynu.cea.fr
- [161] P. Sarriuguren, R. Rodríguez-Guzmán, and L. M. Robledo, *J. Phys. G: Conf. Ser.* **205**, 012024 (2010).
- [162] R. Rodríguez-Guzmán, P. Sarriuguren, L. M. Robledo, and S. Perez-Martin, *Phys. Lett. B* **691**, 202 (2010).
- [163] R. N. Panda and S. K. Patra, *J. Mod. Phys.* **1**, 312 (2010).